An Innovative Method of Measuring the Optical Properties of Tissue

Henry Lehtiniemi and Martin Rupinski

April 4, 2002

Abstract

This paper relates to the field of tissue optics, and in particular to measurement techniques for determining the optical properties in thin slab samples. The principles of an innovative arrangement for extracting the absorption coefficient μ_a, the scattering coefficient μ_s and the anisotropy factor g from combinations of angular and spatial transmittance and reflectance measurements are briefly outlined. The implementation of the evaluation, including set-up, phantoms and measurements, is discussed. Measurements on 24 phantom liquids with optical properties typical of biological media show mean errors of 161%, 85% and 5% in the absorption coefficient, the scattering coefficient and the anisotropy factor.

Contents

1 Introduction

1.1 A Brief Introduction to Tissue Optics

The origins of the scientific field denoted ”Tissue Optics” or sometimes ”Medical Optics” can be found in the problems related to finding a way of thoroughly understanding the underlying mechanisms of light transport in strongly scattering media such as tissue. Within this broadly formulated and perhaps vague problem setting, the central problem can be expressed as the quite tangible problem of finding the best possible way of accurately describing light transport in strongly scattering media.

This description is of tremendous importance when planning the implementation of and analyzing the results from essentially all light based diagnostic medical techniques. Profound understanding of light transport in media such as human tissue is even more important when predicting the most probable result of a light based medical treatment application, such as laser surgery, or when evaluating the results from previously undertaken therapeutic treatments involving laser- or other types of radiation. Tissue optics is a vast and growing interdisciplinary scientific field, involving scientists from a wide range of disciplines, including mathematics, physics, computer science, and medicine.

Ever since its innovation in the middle of the 20^{th} century, the laser has enabled a scientific revolution to take place within the field of light based medicine, and today the laser constitutes an indispensable tool in medicine. The laser is in brief an extraordinary radiation-generating device, the name of which is an acronym of the very physical principle it is based upon - light amplification by stimulated emission of radiation. Furthermore, the laser is characterized by its capacity of producing light with unique properties, notably high intensity, directionality, and monochromacity. With the continuing development of more and more sophisticated lasers and the resulting inevitable increase in numbers of laser based medical applications, tissue optics has experienced a growing interest from the scientific community.

The potential in the heating properties of the laser was recognized early in the history of the laser, and in laser based medical treatment applications, the heating capacity of the laser is exploited. In surgery, the laser can be used as a knife with extraordinary properties: It coagulates blood while it cuts, is absolutely sterile, and provides no mechanical stress. These unique properties in conjunction are particularly desirable when delicate surgery must be performed, as in the case of neurosurgery, where unnecessary bleeding must be avoided, the risk of infection minimized, and the mechanical

stress virtually eliminated.

The high directionality of the produced light is also a characteristic property of the laser. The directionality is of importance in laser based surgery, for instance in laser based eye surgery where the eyes themselves include biological lenses. Laser based eye surgery has evolved from an exotic phenomenon to a proliferated medical treatment technique. Every day, lasers are used around the world to correct myopia, and to photo coagulate excessive blood vessel growth, common in the eyes of diabetes patients.

In contrast to so called black body light sources, the monochromacity of the laser enables treatments based on the fundamental concept of selective absorption. In brief, the principle of selective absorption signifies inducing light into a treatment volume, said light being associated with certain previously defined characteristics in such a way that the absorption in a certain first part of the exposed volume, the target volume, will amount over a certain desired first threshold, while the absorption in a second part of the exposed volume, typically the tissue which is surrounding the target volume is kept below a second threshold. Application of the principle of selective absorption is standard procedure in many laser based therapeutic techniques, and is normally carried out in order to maximize the impact of the radiation in a certain subset of the tissue which is to be destroyed (the target tissue) while minimizing the impact of the radiation in the typically healthy tissue which is surrounding the previously mentioned subset.

In practice, treatments based on the principle of selective absorption involve the following steps: Initially, careful mapping of the optical properties of the tissue which is selected for treatment is carried out. At this stage, the target tissue is normally somehow identified and the scattering and absorption properties are investigated for the target tissue and the surrounding tissue respectively. The following steps consists of spectroscopic analysis of the results, upon which the selection of at least one wavelength, at least one pulse length, and other pertinent properties (such as beam size, energy density et cetera) is based.

The afore mentioned concept enables many interesting therapeutic applications, especially when we consider the case of inducing light associated with a high energy density into a certain, selected target tissue located inside the human body such as a cancerous tumor, in such a way that the absorption in this pre-chosen target tissue is maximized in order to literally evaporate the tumor while the absorption in the surrounding tissue is minimized in order to limit the negative side effects (i.e. burn damage) from the treatment. In many cases, cooling means are applied in parallel with the treatment.

Selective absorption techniques thus enables us to vaporize tumors without harming the surrounding tissue or to perform cosmetic surgery such as removal of port wine stains, tattoos or unwanted hair growth with no or little side effects on the surrounding tissue. The principle of selective absorption is also used in so called spot welding of the retina in cases of retinal detachment, just to mention a few of the applications.

Laser techniques are also used to detect cancer by inducing fluorescence in certain agents, intravenously introduced into the body and absorbed by cancer cells. A part of the scientific progress within the forefront of this particular field has been and is carried out at the medical laser group at

the Department of Physics at Lund University.

We summarize by stating that it is evident that the optical-thermal response of the laser-irradiated tissue must be accurately predicted in all the previously mentioned and other laser based medical techniques. In laser based therapeutic techniques, which are often based on the principle of selective absorption, the optical characteristics of both the target tissue and the surrounding tissue must be carefully mapped. There are a few laser based measurement techniques for doing so and the field of available techniques for determining namely the optical properties in strongly scattering media such as tissue is undergoing constant development.

It is worthwhile to keep in mind that the optimization of the treatment parameters is a process which is founded on an interdependence between on the one hand a mathematical model and on the other hand a set of parameter values. This interdependence implies important limitations to the correspondances of the predicted optimal parameters with the true optimal parameters.

With an absolute correspondance between the mathematical model and the physical reality, the true optimal parameters could have been calculated, but due to the complexity of the situation in almost every practical application, the mathematical model is far from perfect and the exactness of the predicted optimal parameters is limited by said mathematical model.

Furthermore, these predicted optimal parameters (which of course may differ from the true optimal parameters) have been calculated from another set of parameter values, which are typically based on measurements. Any person skilled in the field of scientific measurements will immediately realize that the exactness of these measurement based parameter values is determined by the technique and equipment of the measurements.

1.2 The Optical Properties of Strongly Scattering Media

”Finding the light energy per unit area per unit time that reaches a target chromophore at some position r is the first task of tissue optics.” [1]

Tissue consists of pseudo-chaotically dispersed, various (and *de facto* varying) concentrations of different atoms, ions, and molecules. Mathematically predicting the propagation of laser light in such a complex media is virtually impossible unless necessary simplifications are carried out resulting in the construction of a more reasonable model.

There are a number of approaches to building a mathematical model which can describe light transport in strongly scattering media such as tissue. During the initial considerations the famous, within the field of optics omnipresent dual wave/particle feature of light is normally taken into account. Depending on the situation which is to be modeled, different approaches will be more or less suitable. In media with a somewhat regular structure, typical wave phenomenon as polarization and interference will be present, but in more irregular and complex media it is very difficult to predict or measure these properties and particle based models tend to be more pertinent.

Several methods where light is modeled as photons, i. e. particles associated with certain energy

and certain other characteristics have been developed, and this proliferated approach has a number of advantages as will be discussed in the paragraphs to come. Nevertheless, the wave-properties of light cannot simply be thrown in the waste basket since there are cases where the wave properties of light will be interesting, notably in cases where biological media show a certain structure such as the case of light transport in elongated muscle cells, where the wave properties of light can be used to explain the angular distribution of scattered light. It is thus not possible to claim that there exists one model which is the most accurate and most suitable for modeling all types of light-tissue interaction phenomenons.

In a popular model which is based upon the particle characteristics as discussed above, tissue is regarded upon as an isotropic, homogeneous media associated with bulk absorption and consisting of randomly distributed scatterers. This model has two great advantages. Apart from providing a solid base from which to design and implement numerical calculations predicting the optical-thermal response of laser-irradiation in tissue, it allows tissue to be characterized using only three parameters, which together give an intuitive feeling of the probable optical-thermal response of the tissue in question. These optical properties of tissue are the absorption coefficient μ_a, the scattering coefficient μ_s and the anisotropy factor g.

The absorption coefficient, μ_a, is defined so that the probability of absorption in an infinitesimal distance ds is $\mu_a ds$. The absorption coefficient renders information about the concentration of different chromophores. Typical values of the absorption coefficient in human tissue are 0-2 cm^{-1}.

The scattering coefficient μ_s, is defined so that the probability of a scattering event in an infinitesimal distance ds is $\mu_s ds$. This optical property gives information on the concentration of scatterers and typical values for the scattering coefficient in human tissue are 10-200 cm^{-1}.

The anisotropy factor, or the g-factor, g, is the average expected cosine of angel scattering and defined as

$$g = \frac{\int_{4\pi} p(\hat{s},\hat{s}')(\hat{s}\cdot\hat{s}')dw'}{\int_{4\pi} p(\hat{s},\hat{s}')dw'} \tag{1.1}$$

where s is a unit vector and the phase function of single scattering, $p(s,s')$, expressed in sr^{-1} is defined as

$$\int_{4\pi} p(\hat{s},\hat{s}')dw' = 1 \tag{1.2}$$

These three optical properties can also constitute the elements in functions which in fact are combinations of the three afore mentioned optical components such as the total attenuation coefficient μ_{tot}, which is the sum of the absorption coefficient and the scattering coefficient. The inverse of this complex optical property is denoted the penetration depth of collimated light (δ).

It is worthwhile to keep in mind that all the properties mentioned are wavelength-dependent.

1.3 Measuring the Optical Properties of Tissue

”The second task of tissue optics, which so far has been the most difficult one, is to develop methods by which the absorbing and scattering properties of tissue can be measured.” [1]

There are several ways of measuring the different optical properties of tissue or other strongly scattering media. Measuring the absorption coefficient and estimating the scattering properties in a sample can be done relatively easy using indirect photo-thermal or photometric techniques, which allow simultaneous determination of the absorbed light and the scattered light. Several of these methods suffer regrettably from the great disadvantage of not being able to separate the scattering coefficient and the g factor, instead rendering a complex optical property, the reduced scattering coefficient μ_s', defined as:

$$\mu_s' = \mu_s(1-g) \tag{1.3}$$

Simultaneous determination of μ_a, μ_s and g has so far only been done using direct measurements of light absorbed or scattered by optically thin (single scattering) tissue sections. The probably most known and proliferated set-up for performing these measurements is referred to as the integrating sphere.

The integrating sphere set-up consists of a light source, which can be any available light source but is preferably a Xenon lamp, which is associated with a monochromator which enables wavelength selectivity, a hollow sphere, covered with a material of high reflectivity and attributed with two holes diametrically opposed each other. By placing a detector at a first hole, any light emerging from a second hole, no matter what angle it is propagating in, will undergo multiple reflections inside the integrating sphere until it is incident on the detector and registered.

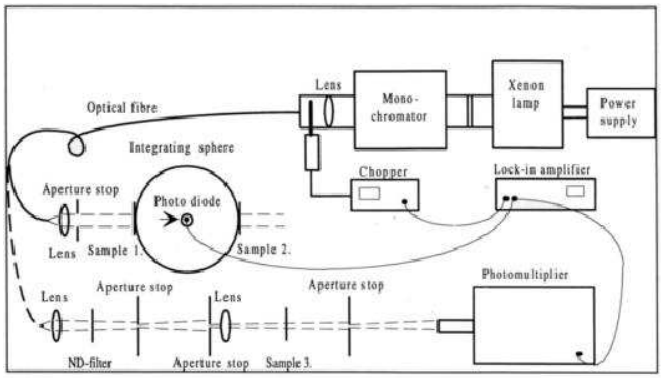

Figure 1.1: Optical scheme of the integrating sphere.

When the integrating sphere is used to measure the optical properties of thin slabs, this is done indirectly by measuring the reflectance, the collimated transmittance and the diffuse transmittance

through the thin slab. This requires two measurements to be undertaken, where the sample is attached to one of the holes, and the light is lead to the sample, preferably by optical fiber means.

The main advantage of the integrating sphere is that it is a set-up, which in fact can be used to extract the three basic optical properties mentioned above and it has been used in a vast number of scientific measurements.

The disadvantages of the integrating sphere set-up are that a sample has to be moved between the measurements, rendering two measurements necessary for each sample and adding a risk for errors during the measurements. The equipment is rather bulky which is another disadvantage, and results are not available in real time. Furthermore, the accuracy in integrating sphere measurements has been discussed.

The field of measurement techniques in tissue optics is an exciting one and new methods are developed constantly. This might owe to the fact that measuring the afore mentioned optical properties is not only useful in diagnostic, therapeutic and other laser-based medical applications but also in quality control in paper manufacturing and various process control applications. Compact, portable and affordable measuring equipment would thus be of great use in several industrial applications.

2 Theory

2.1 Overview of an Innovative Measurement Technique

This diploma project consists essentially of an experimental evaluation of a new technique for measuring the optical properties of strongly scattering media. This technique was suggested by Jan Sørensen Dam et al in ”Monte Carlo study on optical characterization of thin turbid samples using angular and spatially- resolved measurements” [2], and will be briefly explained below.

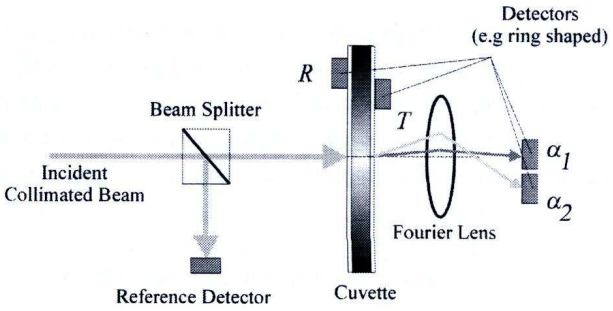

Figure 2.1: Practical realization of configuration D in figure 2.6.

Behold the optical scheme in figure 2.1, where the direction of propagation of light is denoted the main optical axis of the set-up. The collimated laser beam is incident on a beam splitter, where a fraction of the light is deviated and sent into a reference detector used to control the intensity of the laser, since the intensity may fluctuate. The remaining light reaches a cuvette containing a thin sample situated on the main optical axis of the set-up. The spatial reflectance from and the spatial transmittance through the sample can be measured with detectors on both sides of the cuvette holder. The remaining scattered light propagating in an angle relative to the main optical axis can be focused into a detector using a Fourier lens.

The suggested set-up includes a detector which measures the spatial reflectance, another detector which measures the spatial transmittance and two detectors which measure the angular transmittance at two angles relative to the main optical axis. It has been suggested that these four signals can be used to extract the absorption coefficient (μ_a), the scattering coefficient (μ_s) and the anisotropy factor (g).

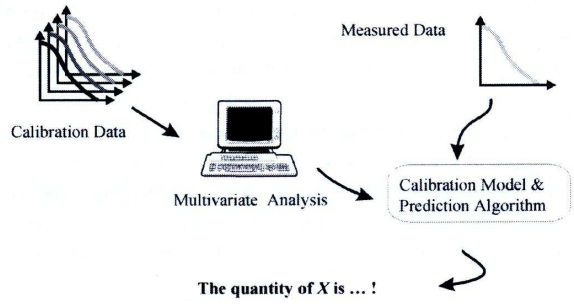

Figure 2.2: Scheme for extracting optical properties using multivariate calibration and analysis.

The following steps are carried out in order to perform extraction of the mentioned optical properties from the signals registered by the detectors:

- Creation of a set of values of μ_a, μ_s and g, and corresponding data from the detectors, within the range of interest for measurements, either by mathematical calculations or by the measurements on phantoms with well defined optical properties.
- Dimension reduction on the set of measured signals from the detectors using Principal Component Analysis (PCA), and creation of a database constituted of on the one hand the principal components of the detector signals and on the other hand the corresponding fundamental optical properties mentioned above.
- Creation of a set of detector data from a sample with unknown optical properties, i.e. measurement on the sample.
- Application of a combined iterative Multiple Polynomial Regression/Newton-Raphson method to the data from the samples and the database, resulting in a prediction of the optical properties of the sample.

2.2 Principal Component Analysis

The mathematical technique referred to as Principal Component Analysis (PCA) was developed in the beginning of the 20^{th} century by among others, Pearson and Hotelling [3]. Due to the complexity of the calculations required, the PCA was during the first half of the 20^{th} century merely a matter of theoretical discussions. The birth and development of powerful numerical instruments i.e. the computer has enabled the PCA to be used in many applications and today, a century later much research is still done within this interesting area.

Principal Component Analysis (PCA) is a ”powerful method to reduce the dimensionality of a data set which consists of a large number of interrelated variables, while retaining as much as possible of the variation present in the data set” [3]. The method consists in constructing a set of N new

variables, Principal Components (PCs), which are uncorrelated linear combinations of the original variables. The PCs are chosen in such a way that most of the variation in the original variables is built into the first PCs. Since these first PCs inherit the important variance from the original variables, the noise in measurements can be assumed to be embedded in the final PC_N.

The principles of deriving the Principal Components are relatively easy to understand. We will illustrate the principles of this method, namely Principle Component Analysis (PCA), with an example on how to calculate the first of these components. In our experiments, dimension reduction using PCA is carried out on four original data variables, which are reduced to three. In order to illustrate the PCA method in the most comprehensible way, we restrict ourselves to the case of reducing three variables into two principle components. The figures have been selected from [6].

We assume that we have three different but interrelated sets of data, for instance data from three detectors. We name these data vectors X1, X2 and X3. A simple plot of these data, would reveal an image which resembles the one below, where the letters a-z may be considered to represent different measurements, i.e. the three data values for a measurement.

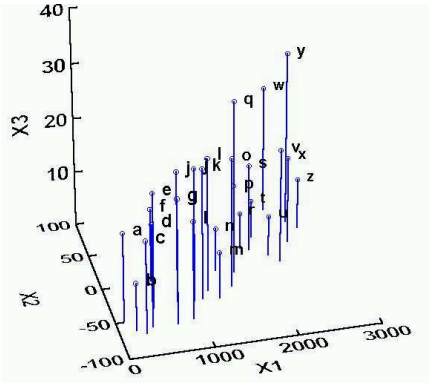

Figure 2.3: Diagram of data from different measurements.

The standardization process which is the initial step in finding the principle components, consists of subtracting the mean and dividing by the standard deviation from the initial data values. This operation transforms the dataset into a new dataset while conserving the internal relationships between the individual datapoints as to their relative position. This may be illustrated with the figure 2.4.

With the data standardized, the gradient representing the greatest variation in the data is found. In the trial illustrated example, the first principle component (PCA 1), clearly is the gradient in which the greatest variation can be found. The following PCA must be chosen in such a way that it is completely uncorrelated to the first PCA while covering the largest variation possible. In the figure 2.5, these two first principle components are drawn (PCA 1 and PCA 2).

For further information on PCA, we recommend Jolliffe's "Principal Component Analysis", Springer-Verlag 1986 [3].

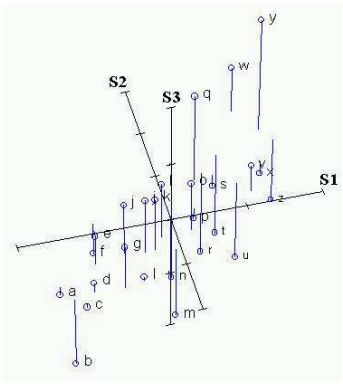

Figure 2.4: Diagram of data after standardization.

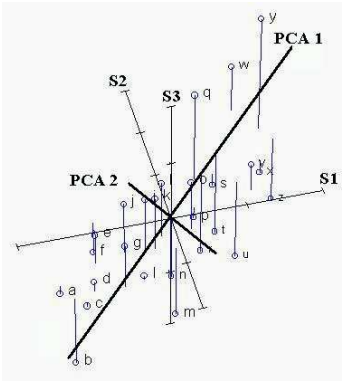

Figure 2.5: Diagram of data, where the first two PCA:s are drawn.

2.3 The Multiple Polynomial Regression/Newton-Raphson Method (MPR-N/R)

The Multiple Polynomial Regression/Newton-Raphson Method (MPR-N/R) used to extract the optical properties includes two steps.

First, a three-dimensional multiple polynomial regression method is applied including the following two steps:

1) Selection of relevant detector data $X_{1-3,cal}$ from the database and finding triple-polynomial fits $X_{1-3,fit}$ to these data in accordance with the equation below, where the fitting coefficients in the matrixes A, B and C are determined by least-squares regression. Thus $X_{1-3,fit}$ constitute the calibration model.

$$\begin{bmatrix} X_{1,fit} & X_{2,fit} & X_{3,fit} \end{bmatrix} = \begin{bmatrix} 1 & \mu_a & \mu_a^2 & \mu_a^3 \end{bmatrix} \times \mathbf{A} \cdot \begin{bmatrix} 1 & \mu_s & \mu_s^2 & \mu_s^3 \end{bmatrix} \mathbf{B} \cdot \begin{bmatrix} 1 & g & g^2 & g^3 \end{bmatrix} \mathbf{C} \tag{2.1}$$

2) Solving the inverse problem of determining μ_a and μ_s' from recordings of the measured data:

$$\begin{aligned} F(\mu_a, \mu_s, g) &= X_{1,fit} - X_{1,meas} \\ G(\mu_a, \mu_s, g) &= X_{2,fit} - X_{2,meas} \\ H(\mu_a, \mu_s, g) &= X_{3,fit} - X_{3,meas} \end{aligned} \tag{2.2}$$

Finally, converging iterative calculations of μ_a, μ_s and g are performed using the Newton-Raphson Algorithm in accordance with the equation below, where the h-terms are the correction terms of μ_a, μ_s and g. The calculations stop when the h-values end up below predefined values.

$$\left.\begin{aligned} -\begin{bmatrix} F(\mu_{a,k}, \mu_{s,k}, g_k) \\ G(\mu_{a,k}, \mu_{s,k}, g_k) \\ H(\mu_{a,k}, \mu_{s,k}, g_k) \end{bmatrix} &= \begin{bmatrix} \frac{\partial F}{\partial \mu_a} & \frac{\partial F}{\partial \mu_s} & \frac{\partial F}{\partial g} \\ \frac{\partial G}{\partial \mu_a} & \frac{\partial G}{\partial \mu_s} & \frac{\partial G}{\partial g} \\ \frac{\partial H}{\partial \mu_a} & \frac{\partial H}{\partial \mu_s} & \frac{\partial H}{\partial g} \end{bmatrix} \begin{bmatrix} h_{a,k} \\ h_{s,k} \\ h_{g,k} \end{bmatrix} \\ \begin{pmatrix} \mu_{a,k+1} \\ \mu_{s,k+1} \\ g_{k+1} \end{pmatrix} &= \begin{pmatrix} \mu_{a,k} \\ \mu_{s,k} \\ g_k \end{pmatrix} + \begin{pmatrix} h_{a,k} \\ h_{s,k} \\ h_{g,k} \end{pmatrix} \end{aligned}\right\} \tag{2.3}$$

$k = 0, 1, 2, 3, 4, ...,$

2.4 Computer Simulations

The suggested set-up, previously described in paragraph 2.1, is the result of theoretical investigations of the possibility of constructing a set-up which using a finite number of detectors measures combinations of light emerging from a cuvette. The spatial transmittance, spatial reflectance and angular transmittance can be measured in combinations allowing the optical properties to be extracted from the data.

In a paper by Jan Sørensen Dam [2], four different set-ups were investigated. These set-ups, displayed below, each use different combinations of detectors which measure spatial and/or angular transmittance and/or reflectance. In this paper, the set-up which we have described in section 2.1 turned out to be a suitable one for performing measurements on properties of thin turbid samples.

These setups were evaluated regarding their performance characteristics concerning a set of values typical of biological media. This evaluation was performed in the following way:

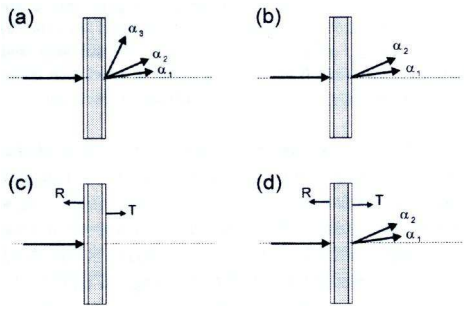

Figure 2.6: Four different set-ups for predicting optical properties.

First, a database was created by performing Monte Carlo simulations using 10^6 photons on a set consisting of combinations of 21 values of μ_a, 19 values of μ_s and 11 values of g - all these values within the typical range of biological media:

$$\begin{aligned} 0 < \mu_a < 2\,cm^{-1} \\ 10 < \mu_s < 200\,cm^{-1} \\ 0.85 < g < 0.99 \end{aligned} \tag{2.4}$$

The following assumptions were made:

- A glass cuvette, with the thickness of walls set to 1.0 *mm*.
- A thin slab sample with thickness set to 1.0 *mm*.
- Refractive indexes: 1.49 for glass, 1.33 for the sample, and 1.00 for the surrounding media.

During each of these simulations, the following data was recorded:

- The spatially resolved diffuse reflectance R as a function of the radial distance $R(r)$.
- The spatially resolved diffuse transmittance T as a function of the radial distance $T(r)$.
- The angularly resolved total transmittance α as a function of the deflection angle θ and the acceptance angle ϕ.

Values obtained from these simulations were inserted into a database which thus contains μ_a, μ_s, g and corresponding values of R, T and α. A calibration was carried out by applying Multiple Polynomial Regression in conjunction with a Newton-Raphson method to the data (R, T and α) as described in paragraph 2.3. The coefficients were calculated using standard least squares optimization.

Next, 20 combinations of randomly chosen values of μ_a, μ_s and g were selected (all these values within the typical range of biological media as displayed above).

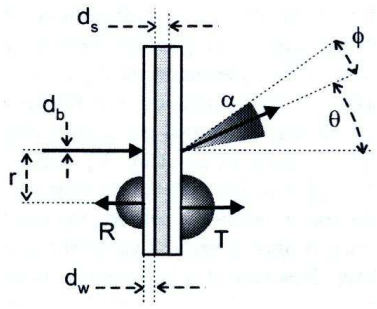

Figure 2.7: Geometric configuration of set-up.

Monte Carlo Simulations were carried out using 10^7 photons for each simulation. In each of the four cases, the optimal combinations of angles and/or distances were chosen, with the optimal combination defined as the combination in which the prediction errors were minimized.

In the fourth set-up, four output signals were obtained. Since the MPR/N-R method requires three input variables, Principal Component Analysis was applied to the output variables to obtain dimension reduction.

The prediction errors obtained for the set-up which we have described in section 2.1 are presented in table 2.1.

Table 2.1: Optimum angles and distances of the four set-ups in figure 2.6

	Angles $\theta(^\circ)$			Distances r (mm)	
	α_1	α_2	α_3	T	R
(a)	0	3	60	-	-
(b)	0	3	-	-	-
(c)	-	-	-	0.7	2.0
(d)	0	5	-	2.0	2.5

3 Method

3.1 Set-up

Our set-up is mounted upon a small ($25 \times 25\,cm$) Melles-Griot optical table, and consists of a 10 mW Melles-Griot HeNe laser ($\lambda = 632,8\,nm$), a set of Melles-Griot microbench components including a Fourier lens ($f = 100\,mm$), lens holders, alignment bars *et cetera*, and five Siemens detectors (Silicon PIN Photodiode BPW34 with a photosensitive area of 2.65×2.65 *mm*) connected via a National Instruments PCI Card to an Acer laptop computer (Pentium 75 Mhz processor) which runs on Windows 95, with LabVIEW 5.0 and MATLAB 5.1 installed.

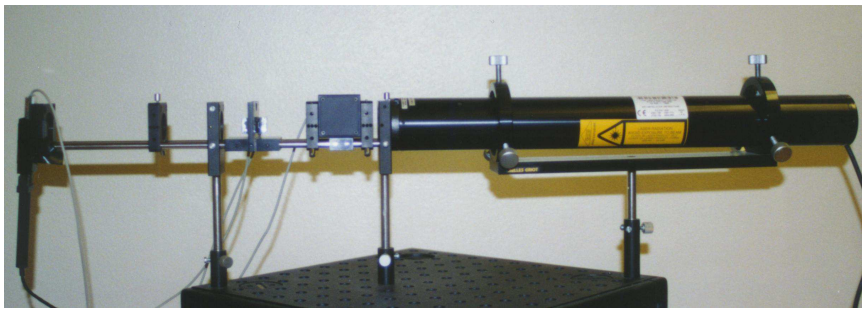

Figure 3.1: Overview of the entire set-up.

In addition to these components, our set-up includes a cuvette holder, designed by us and custom manufactured at the fine-mechanical workshop at the Department of Physics, Lund Institute of Technology. The cuvette holder was made of aluminum and made black using chemical processes in order to minimize the risk for reflections from its surface. The cuvette holder measures 40x20x5 mm and has been designed to assure compactness of the equipment, compatibility with microbench components, easy manufacturing, and user friendly operation.

The cuvettes were made by us using 1 mm thin transparent standard laboratory slides. They hold approximately 400 microliters in a 1 mm thick rectangular compartment and were designed to be compatible with the integrating sphere equipment at the Department of Physics, Lund Institute of Technology.

Although several cuvettes were manufactured, only one of them was used in the measurements

performed by us. This to eliminate the possible error source inherent from the minor discrepancies in the dimensions of the cuvettes.

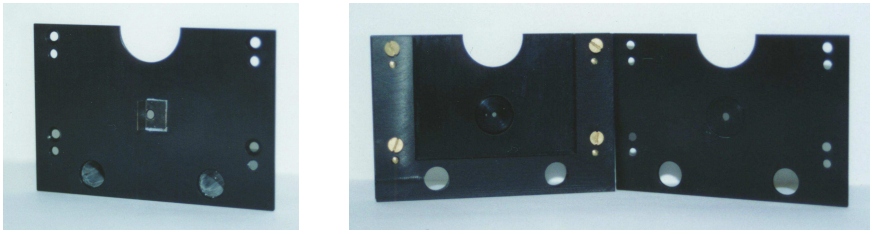

Figure 3.2: Close view of cuvette holder.

The software includes a data acquisition program written in LabVIEW and a series of programs written in MATLAB, which use a data base with Monte Carlo simulated values of the spatially and angularly reflected and transmitted light for specimens having optical properties typical of human tissue.

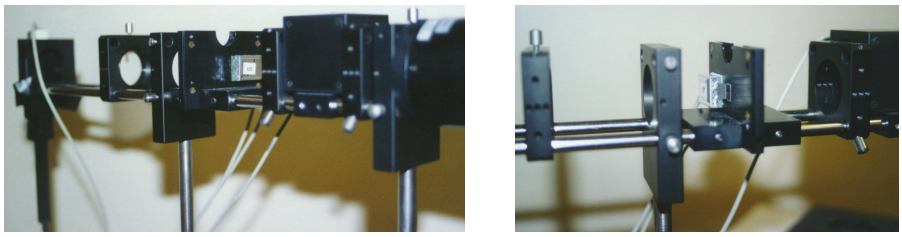

Figure 3.3: Location of the detectors on the cuvette holder.

The mode of operation is illustrated in figure 2.1. The light emerging from the HeNe laser passes through a beam splitter, where 50% of the light is deviated in a 90 degree angle into a reference detector and the remaining 50% is transmitted in an unaltered fashion. The light subsequently enters the small entrance hole of the cuvette holder and impinges on the contained cuvette, where it is scattered by the contents.

A detector registers the backscattered light at 2.0 mm from the center of the entrance hole, and another detector registers the light transmitted in parallel with the optical axis 2.5 mm from the center of the entrance hole. The light emerging from the exit hole is diffracted by a Fourier lens ($f = 100\,mm$) in such a way that the light transmitted from the cuvette holder in a 0 degree angle relative to the optical axis is detected by one detector while the light transmitted from the cuvette holder in a 5 degree angle is detected by another detector. The signals from the detectors are finally sent via a PCI-card into the portable computer .

The distances and the angles, which have been selected for the detectors are the optimal ones presented in a paper by Jan Sørensen Dam [2].

Data acquisition is carried out using a LabVIEW program, which produces output in the form of a

spreadsheet file, the columns of which are the detector signal.

Provided that calibration has been undertaken, the spreadsheet file can be used as input data to a MATLAB program, which in accordance with the principles described in the theory section processes the data, references to a data base of Monte Carlo simulated values, and iterates producing the calculated values of μ_a, μ_s and g.

3.2 Manufacturing of Phantoms

A total of 150 phantoms were manufactured for the evaluation process, each phantom having optical properties within the range of biological media as stated in the theory section.

Initially, ten solutions with absorption coefficients ranging from 0.20 to 2.00 cm^{-1} in steps of 0.20 cm^{-1} were manufactured by dissolving green household dye produced by Ekströms in distilled water. The wavelength used was 632.8 *nm* and the absorption coefficients were measured using 10 *mm* thick glass cuvettes in a dual-beam Perkin-Elmer Lambda 3B Spectrophotometer at the Department of Analytical Chemistry, Lund University. Distilled water was used as a reference, i.e. the absorption through an identic 10 *mm* thick glass cuvette containing distilled water was set to zero.

The absorption coefficients of these solutions were measured again a week later, this time using a single beam Hitachi U-1100 Spectrophotometer at the BioMedical Centre (BMC), Lund University. The solutions were poured into sample tubes containing 1200 microliters each and homogenous latex microspheres (Bangs Labs) were subsequently added in concentrations of 1.0-10.0 micro liters resulting in phantoms having scattering coefficients of 10, 50, 100, 150 and 200 cm^{-1}. The scattering coefficient in water was assumed to be zero and the addition of microspheres was assumed to have no or negligible impact on the absorption coefficients. The scattering coefficients were calculated using Mie theory.

The procedure of adding microspheres was effectuated using homogenous latex microspheres of three different sizes corresponding to g=0.87, g=0.91 and g=0.93. In this way, 150 phantoms (linear combinations of the discrete values of the absorption coefficient, the scattering coefficient and the g-factor below) were manufactured.

$$\begin{aligned} \mu_a &= \left\{ \begin{array}{cccccccccc} 0.2 & 0.4 & 0.6 & 0.8 & 1.0 & 1.2 & 1.4 & 1.6 & 1.8 & 2.0 \end{array} \right\} \\ \mu_s &= \left\{ \begin{array}{ccccc} 10 & 50 & 100 & 150 & 200 \end{array} \right\} \\ g &= \left\{ \begin{array}{ccc} 0.87 & 0.91 & 0.93 \end{array} \right\} \end{aligned} \tag{3.1}$$

3.3 Measurements

Measurements were carried out using only our hybrid angular / spatial set-up. Measurements made using the integrating sphere set-up at the division of Atomic Physics, Lund Institute of Technology

prior to the measurements with our set-up for a subset of the phantoms, were dismissed due to malfunction of the integrating sphere equipment relating to deficiencies in the cooling apparatus of the CCD camera. Due to risk of deterioration in the phantoms, the measurements were carried out using only our equipment, since the absorption properties had been carefully investigated, and the scattering properties had been carefully calculated using reliable software [4].

At an early stage in the development phase, the detector measuring the angular transmittance at zero degrees was found to be inadequate with respect to the range of the detector, since the range of the values of the transmitted intensity at this angle was larger than the sensitivity range of the detector in question. On instructions from the Bang&Olufsen project representative and after consultation with the department responsible, the decision to replace the failing detector with a photometer was taken. The advantage with this modification was that it permitted us to measure the transmitted intensity at zero degrees. A disadvantage with this modification was that no appropriate way of transmitting the detector data from the photometer into the computer was at our disposal. During the measurements, the photometer was programmed to produce average values of the intensity over a period of 3 seconds, and these average values were read and inserted into the computer manually.

In order to eliminate the error source related to the potential discrepancies in size, shape *et cetera* in the hand made cuvettes, the decision was made to carry out the measurements using only one (1) cuvette, which was carefully cleaned between the measurements.

The phantoms were initially agitated in order to disperse the microspheres present in the phantoms. The measurements were carried out by introducing each of the phantoms into the cuvette, previously rinsed with distilled water and dried. The cuvette was lowered into the cuvette holder in our set-up and the measurements were undertaken in virtually complete darkness in the laboratories at the division of Atomic Physics.

The data acquisition consisted of 1000 measurements during one (1) second. All measurements were performed during a total of two subsequent days in order to eliminate the risk of deterioration or change of other kind in the phantoms.

The data from the operating detectors were instantly input via the software into our computer using the LabVIEW-software and the output was in the form of a spreadsheet file, to which the data from the photometer was added.

Of the 150 phantom measurements, 24 were selected as suitable for evaluation purposes, since these values represented combinations of μ_a, μ_s and g, where interpolation was possible i.e. none of the optical properties in these phantoms represented an extreme value.

For each of these 24 phantom measurements, a calibration model was determined using the remaining 149 phantoms, and predictions of the optical properties of these phantoms were calculated in accordance with the methods described previously in the theory section.

4 Results

Predictions of the optical properties of the 24 phantom liquids, calculated using the method described in the previous chapter, are accounted for in the following. The consistence of the measured values with the experimental values of the absorption coefficient and the theoretical values regarding the scattering coefficient and anisotropy factor respectively are summarized in the paragraphs below.

The absorption coefficient μ_a shows a mean error of 161% from the experimental values obtained from the Perkin-Elmer Lambda 3B Spectrophotometer at the Department of Analytical Chemistry, Lund University.

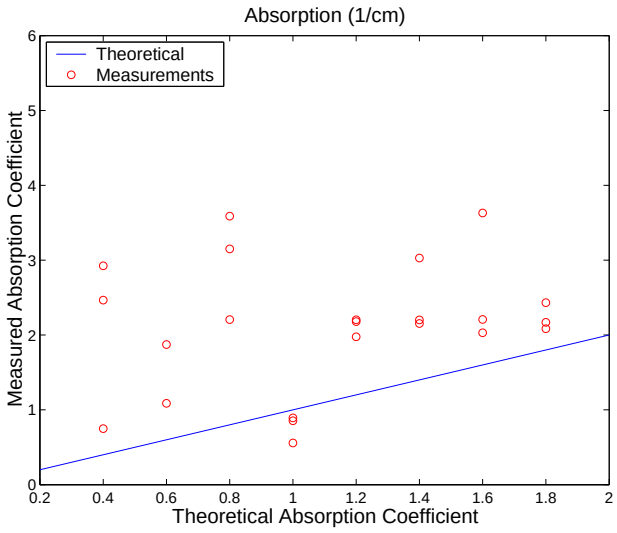

Figure 4.1: Diagram of theoretical and prediction values of μ_a.

The scattering coefficient μ_s shows a mean error of 85% from the theoretical values obtained from the Mie-calculations performed using previously mentioned software [4].

The anisotropy factor g shows a mean error of 5% relative to the theoretical values obtained from the Mie-calculations performed using previously mentioned software [4].

Additional data analysis on the collected data was carried out by researchers at Bang&Olufsen, but no predictions could be made on the data due to its high level of noise.

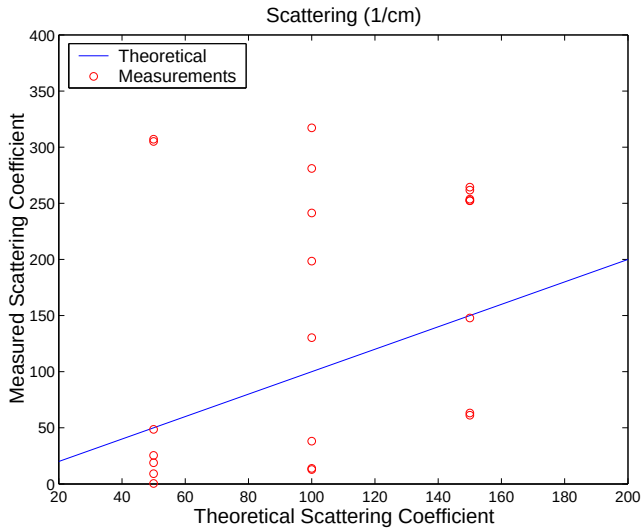

Figure 4.2: Diagram of theoretical and prediction values of μ_s.

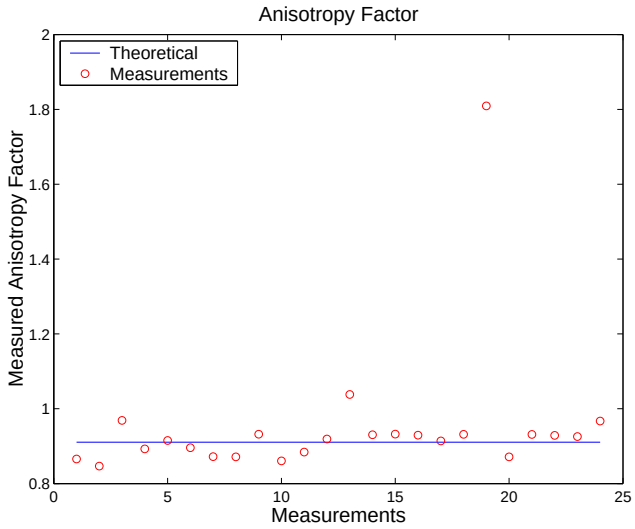

Figure 4.3: Diagram of theoretical and prediction values of g.

5 Discussion

5.1 Error Sources Related to the Set-up

The set-up which was designed by us is attributed with a number of possible sources of errors relating to the measurements. These errors will be discussed and suggestions on how to improve the system will be given in the following paragraphs.

The optimal set-up includes detectors placed at certain distances, and a lens and a beam splitter placed at certain other distances relative to the thin slab sample. During manufacturing of the set-up, the locations of the holes and the location of the lens and beam splitter were checked several times, and prior to the measurements, the locations of the holes and the detectors along with the specific locations of the rest of the optical equipment included in the set-up were measured using a micrometer and found to correspond exactly to the values specified in the paper by Jan Sørensen Dam [2] .

During initial design considerations, the idea of including fibers as light conducting means from the thin sample to the detectors was rejected, due to the fact that such a design would constitute a far greater design effort than what was reasonable for an initial evaluation. The great advantage with such a set-up would have been a dramatic reduction in scattered light.

The characteristics of the detectors used in the set-up were not satisfactory for the signal from the angular transmittance for zero degrees, due to the fact that the range of this signal exceeded the range of the detector. This problem was dealt with in the somewhat primitive way of simply removing the detector and instead attaching a photometer in its place. The read-out from the photometer had to be read and manually inserted into the spreadsheet files containing data to be processed.

5.2 Errors Related to the Manufacturing of the Phantoms

Several measures were undertaken in order to minimize the risk for errors in the manufacturing of the phantoms. The green household dye dissolved in double-distilled water was chosen, since it had been used previously to induce absorption in liquid phantoms. The procedure for providing absorption in a liquid in this way was thus the recognized and state of the art way of doing so, and

the reliability of such phantoms as to change in the absorption properties over time was considered to be high.

The absorption properties of the liquids were further on thoroughly verified experimentally - first using a Perkin-Elmer Lambda 3B spectrometer at the department of analytical chemistry and a week later, prior to the measurements using a Hitachi U-1100 spectrometer at Biomedical Centre, Lund University. We are thus convinced that the absorption properties of the phantoms were indeed consistent with the desired, theoretical values.

We did not have any method of investigating the properties in the scatterers, i.e. the microspheres from BangsLabs to our disposal, but since these were kept in a refrigerator and the measurements were undertaken just a few months from the manufacturing of the latex microspheres themselves, we trust the word of the manufacturer and assume the risk of error in the microspheres to be infinitesimal. Furthermore, investigation of the microspheres indicated that these seemed fresh and no agglutination or sedimentation was detectable with the human eye.

The proportions in which the microspheres were added to the dye/distilled water solutions were thoroughly calculated using a standard software [4]. The resulting calculations were checked and double checked.

5.3 Error Sources Related to the Measurements

Finally, the error sources related to the measurements themselves will be identified and discussed in these final paragraphs.

Several potential error sources relating to the measurements were recognized during the measurements and adequate measures were taken to minimize the impact from these. The measurements were carried out in virtually complete darkness, not only in a laboratory with blinds, but also the instrumental lights from the computer screen and from various indicator lights on the equipment were covered during the measurement to virtually annihilate stray light.

The phantoms themselves were carefully labeled, and a double protocol was kept during the measurements. When the slightest doubt concerning the identity of the sample in the cuvette arose, the results were immediately rejected and the measurements were performed again. This occurred twice during measurements on a total of 150 phantom liquids. Thus we are certain that we haven't committed any errors such as mixing up the phantoms.

Finally, the error arising from the inaccuracies in the read-out from the photometer must be mentioned. This read-out was found to fluctuate (as was the case for the signals from the rest of the detectors as well), and in order to find a correct way of measuring the noisy signal, the instrument was programmed to average the results over a time period of 3 seconds. Since the results from the detectors consist essentially of the averaged values of in all 1000 measurements during 1 second, we find that this way of eliminating the risk for error in reading the output from the photometer was a good one.

5.4 Suggestions for Improvements

The presented results and the previous discussions serve as starting points for further discussions concerning suggestions for improvements regarding the realization of the present method. These suggestions are summarized in the following paragraphs, and are intended to assist future developers of alternative embodiments of the invention by providing our reflections from the experiences we have made during the design of the equipment, the measurements and the data analysis.

The very first improvement suggestion relates to the use of the photometer as a substitute for a detector during the measurements. It is evident that a more preferred embodiment of the set-up would have included detectors capable of producing reliable measurement data when measuring intensities which vary within a rather large interval, as was the case with our set of phantoms. Nevertheless, we do not believe that this feature has constituted the largest error source in our measurements, due to the reliability of the photometer, but merely a less elegant and perhaps quick solution to a measurement problem.

Considering the set-up as a whole, the positioning of the lens and the isolation of the light emerging in distinct angles from the exit hole of the cuvette have proven to be quite demanding from a construction point of view. There were difficulties relating to the selection of light emerging in a small angle from the exit hole. Future constructors should consider using fibers.

The risk of noise from stray light is inherent with the open positioning of the detectors both on the cuvette holder and more notably on the detector plate following the lens. Our suggestion to an improvement considering this aspect of the set-up would be to use fibers when isolating the light and sending it to the detectors. The use of fibers would allow the angular selection of the light to be more accurate and furthermore clearly reduce the risk for stray light related disturbances.

It is also possible to imagine a set-up using more than four detectors. From a data acquisition point of view, this should not impose any problem to modern computers and electronics. With an increasing number of signals, it would be possible to diminish the errors from noise.

6 Conclusions

This first evaluation of an innovative measurement technique for simultaneous real time determination of the optical properties of strongly scattering thin slab samples has not proven to demonstrate the accuracy which we would have expected given theoretical simulations.

Measurements on 24 phantom liquids with optical properties typical of biological media show mean errors of 161%, 85% and 5% in the absorption coefficient, the scattering coefficient and the anisotropy factor.

Nevertheless it is worth to mention that we have been able to identify a number of potential error sources, and provided that these error sources can be excluded - for instance by using fibers as described earlier, or by modifying the set-up and adding detectors, the possibility of a successful implementation on the theoretical principles cannot be ruled out.

Bibliography

[1] A.J. Welch, M.J.C. van Gemert, W.M. Star and B.C. Wilson. *Optical-Thermal Response of Laser-Irradiated Tissue.* Plenum Press, New York, NY, 1995 .

[2] Jan S. Dam, Carsten B. Pedersen, Torben Dalgaard, Paul-Erik Fabricius and Stefan Andersson-Engels. *Monte Carlo Study on Optical Characterization of Thin Turbid Samples Using Angular and Spacially-resolved Measurements.* Included in ”Optical Analysis of Biological Media - continuous wave diffuse spectroscopy”, Doctoral Thesis, Lund Institute of Technology, 2000. ISBN 91-628-4546-2.

[3] I.I. Jolliffe. *Principal Component Analysis.* Springer-Verlag New York Inc., 1986. ISBN 0-387-96269-7.

[4] L-H Wang, S.L. Jacques, L-Q Zheng. *MCML - Monte Carlo modeling of photon transport in multi-layered tissues.* Computer Methods and Programs in Biomedicine 47:131-146, 1995.

[5] C. Eker. *Optical characterization of tissue for medical diagnostics.* Doctoral Thesis, Lund Institute of Technology, 1999. ISBN 91-628-3889-X.

[6] Michael Palmer, *http://www.okstate.edu/artsci/botany/ordinate/PCA.htm*.